
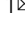




The Horseshoe Abyssal plain Thrust could be the source of the 1755 Lisbon earthquake and tsunami

Sara Martínez-Loriente ¹, Valentí Sallarès ¹ & Eulàlia Gràcia ¹

The southwest Iberia margin is widely believed to have hosted the 1755 Great Lisbon earthquake and ensuing tsunami, one of the most destructive natural events in European history. Here we combine geophysical data and numerical tsunami modelling to investigate the source and mechanism responsible for this event. We find that an intra-plate, lithospheric-scale thrust fault located at the Horseshoe Abyssal Plain coincides with the location and focal mechanisms of the largest regional earthquakes and is likely to have suitable dimensions and fault-rock properties to account for the magnitude of the 1755 event. We present tsunami simulations with this fault as the source, and find that they reproduce reported tsunami energy propagation patterns, arrival-times and run up heights more successfully than other modelled sources. We propose that a reverse dip-slip mechanism on the northwest verging Horseshoe Abyssal plain Thrust, combined with the two-state mechanical behaviour of serpentinite, is the most likely candidate for the source of the 1755 Great Lisbon earthquake and for other recent large regional earthquakes.

¹Institut de Ciències del Mar, ICM-CSIC, Barcelona, Spain. ✉email: smartinez@icm.csic.es

The present-day Eurasia-Africa plate boundary off southwest Iberia is dominated by a northwest (NW)–southeast (SE) trending convergence (3.8–5.6 mm yr⁻¹)¹ (Fig. 1). The plate boundary is diffuse² and deformation is accommodated along a 600 km-long deformation band² by a series of thrust and strike-slip faults^{3,4}. It is one of the most seismically active regions in Western Europe, showing a constant background of seismic activity with low to moderate magnitude events of up to magnitude (M_w) ~ 6.0^{5–8}, mostly concentrating at upper mantle depths^{6–8}. Besides the background seismicity, this area has also experienced large magnitude events in historical and instrumental times, such as the 1755 Lisbon (estimated M_w 8.5+)^{9–14} and the 1969 Horseshoe (M_w 7.9)¹⁵ ones.

The 1755 Great Lisbon earthquake has the largest documented felt area of any shallow earthquake^{9,16}. The ground motion was felt as far away as Hamburg, Great Britain, the Azores and Cape Verde Islands⁹, producing a remarkable agitation of lakes, rivers and harbours in a rhythmic way as far as Great Britain, Switzerland, Finland and Sweden^{17,18}, and it was one of the most destructive known earthquake in European history¹⁹. The associated tsunami, with run-up heights reported to reach 5–15 m¹⁵, devastated the coasts of SW Iberia and NW Morocco. The event is thought to have caused near 20,000 victims¹⁰ combining the effects of ground-shaking, the related fires and ensuing tsunami, which were reported to hit as far as England, Newfoundland, the Caribbean and Brazil¹⁹. Given such evidence, the scientific community widely supports an estimated $M_w \geq 8.5$ ^{9–14} for the Lisbon earthquake, although a recent work has also suggested a lower magnitude²⁰. The source and the generating mechanism

of the Lisbon earthquake have been the subject of numerous studies and the matter of a continuous debate during the last decades^{5–29}. A number of candidate sources have been proposed^{11,22–28}, although none of them explains satisfactorily the inferred seismic moment of the event, as well as the arrival times and, particularly, the run-up heights of the tsunami referred to in historical reports.

The southwest Iberian margin has undergone a complex geodynamic history spanning from the Mesozoic extension to the Neogene-to-present-day convergence. Martínez-Loriente et al.³⁰ used P-wave seismic tomography models obtained along two regional controlled-source wide-angle seismic profiles (profiles P1 and P2 in Fig. 1), to show the presence of three different oceanic domains in the area originated in three different opening systems (Fig. 1a). First, the Seine Abyssal Plain (SAP) domain, which is made of oceanic crust generated during the first stages of seafloor spreading in the NE Central Atlantic (Early Jurassic). Second, the Gulf of Cadiz (GC) domain, formed by Jurassic-age oceanic crust generated at the Alpine-Tethys oblique-spreading system between Iberia and Africa (i.e., the Western Tethys)³¹. Third, the Gorringe Bank (GB) domain, composed of unroofed mantle rocks with little synchronous magmatism. These rocks, which constitute the basement of the GB, southern Tagus and northern Horseshoe Abyssal plains (HAP), were exhumed during the first stages of North Atlantic opening (Lower Cretaceous)³². The present-day plate configuration was established ~20 Ma ago, when the plate boundary between Africa and Eurasia shifted from north to south Iberia³³ (Fig. 1b). The Neogene NW–SE convergence resulted on the emplacement of large allochthonous masses during the

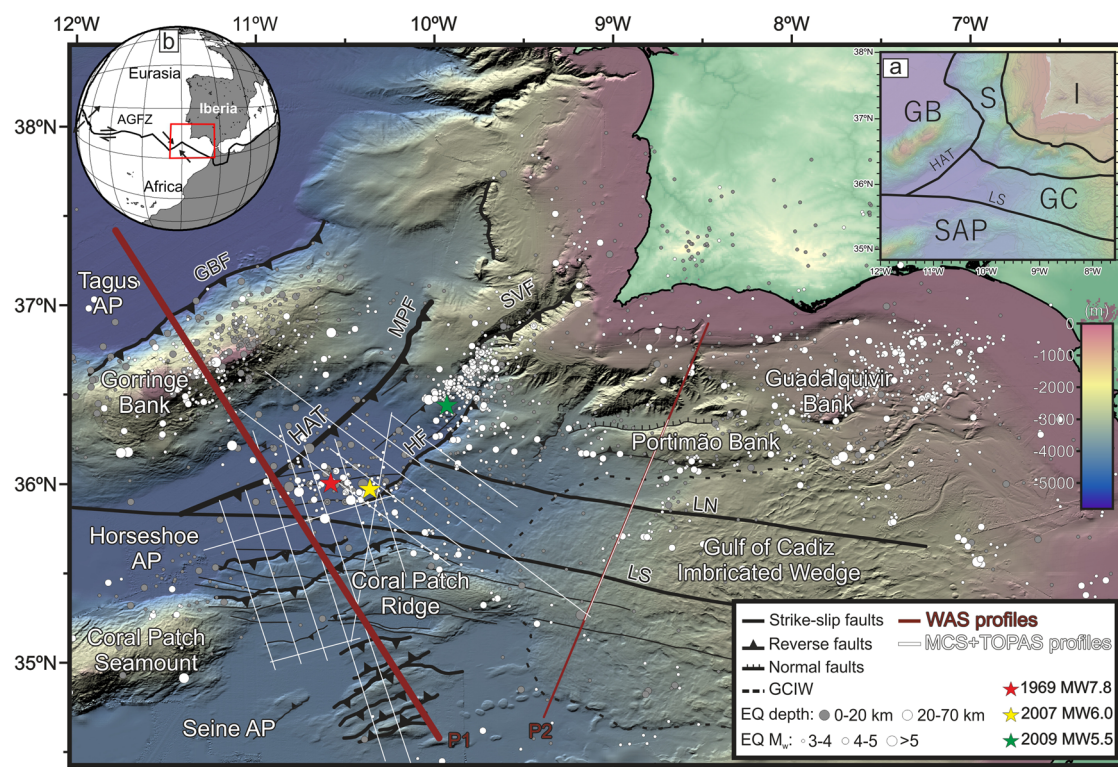


Fig. 1 Tectonic map offshore SW Iberia. Bathymetric map of the SW Iberian margin with the location of the main active tectonic structures⁴. The thick brown line is the wide-angle seismic profile P1³⁰ along which the schematic cross-section of Fig. 2 has been drawn. The stars indicate the largest instrumental earthquakes that have occurred in the region (i.e., 1969¹⁵, 2007⁵, 2009³⁸; Supplementary Table 1). White and grey circles show epicentral locations of regional earthquakes with $M_w > 3$ for the period 1960–2020⁵⁷. **a** Map of the SW Iberian Margin Geological Domains³⁰. **b** Global map including the major tectonic plates and boundaries. The red rectangle corresponds to the area depicted in this figure. AGFZ: Azores-Gibraltar Fault Zone; AP: Abyssal plain; GBF: Gorringe Bank Fault; HAT: Horseshoe Abyssal plain Thrust; HF: Horseshoe Fault; LN: Lineament North; LS: Lineament South; MPF: Marquês de Pombal Fault; SVF: São Vicente Fault.

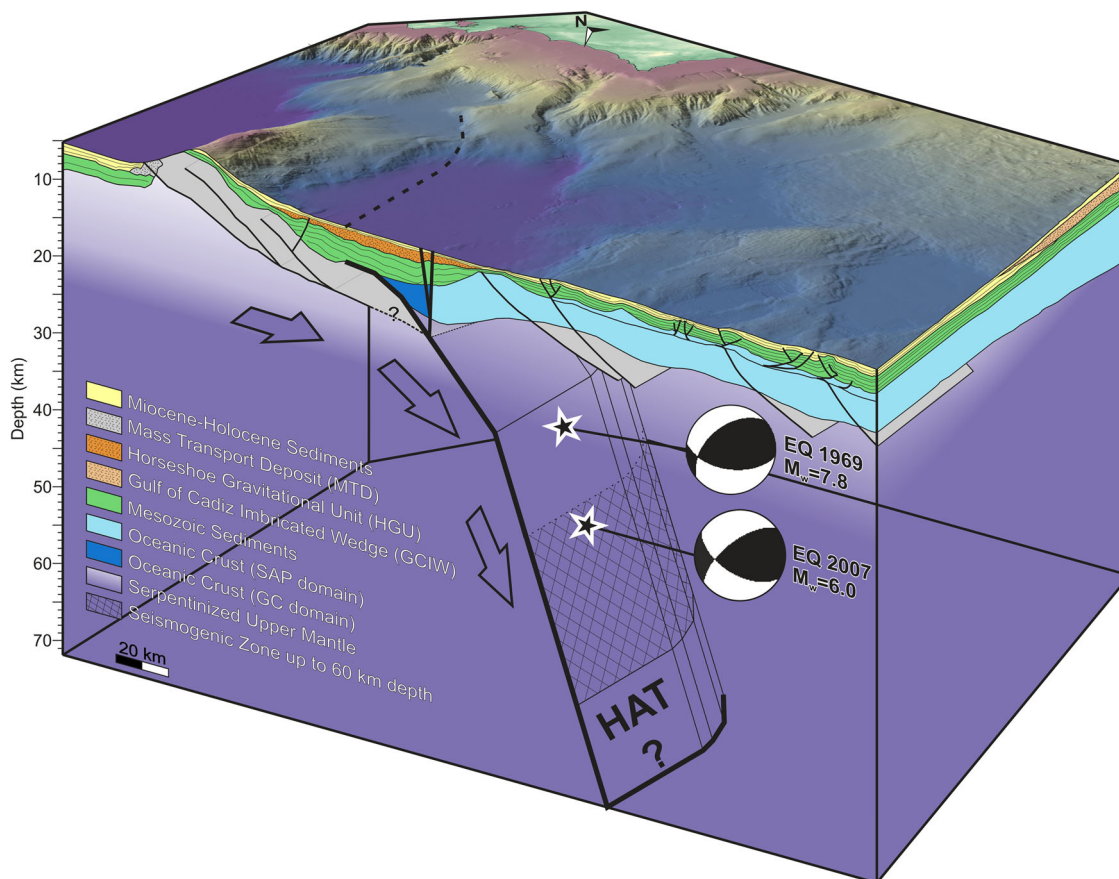


Fig. 2 The Horseshoe Abyssal plain Thrust (HAT) 3D scheme. The 3D regional tectonic and stratigraphic cross-section along profile P1 (located in Fig. 1) showing the geometry of the HAT and the projection in depth of the 1969 M_w 7.9^{15,37} and 2007 M_w 6.0^{5,38} earthquakes (Supplementary Table 1). Serpentinization degree is indicated as gradation of colour.

Tortonian³⁴ and caused the reactivation of major Mesozoic extensional faults³. These data also allowed identifying the presence of the Horseshoe Abyssal plain Thrust (HAT), a deep thrust fault located in the HAP, away from any well-established subduction zone.

The deformation resulting from the present-day NW–SE convergence ($3.8\text{--}5.6\text{ mm/yr}$)⁻¹ is mainly accommodated by two types of active faults. The first includes regional NE–SW trending thrusts, such as the HAT³⁰, the GB Fault (GBF)^{9,32} or the Marquês de Pombal Fault (MPF)^{24,25}, whereas the second comprises large west northwest-east southeast trending dextral strike-slip faults (i.e., the South West Iberian Margin (SWIM) faults)²⁸, such as the so-called Lineaments North and South^{3,35,36} (LS) (Fig. 1). According to Martínez-Loriente et al.³⁰, the SAP and GC oceanic basement domains are separated by the LS strike-slip fault, whereas the GC and GB domains are limited by the HAT. This means that the HAT separates exhumed mantle rocks (NW) from oceanic lithosphere (SE) (Figs. 1 and 2).

In this work, we show that the HAT has the dimensions, geometry, and fault-rock bulk properties required to explain the deep regional seismicity, and that it has the potential to generate earthquakes as large as the 1755 Lisbon one. In addition, we have performed tsunami simulations to show that the HAT source can generate transatlantic tsunamis with characteristics compatible with those referred in historical records of the 1755 event. Finally, we discuss the regional and global implications linked with the presence of this deep thrust and the bulk-rock properties in terms of seismic and tsunami hazard assessment.

Results and discussion

Origin of deep seismicity offshore SW Iberia. The seismic activity in the study area mostly concentrates north of the LS, between the Gorringer and Guadalquivir banks (Fig. 1). Regional micro-seismicity recorded by temporal networks of Ocean Bottom Seismometers (OBS)^{6–8} has allowed identifying three main seismicity clusters located in the GB, HAP, and Sao Vicente Canyon (SVC)⁸ displaying a combination of thrust and strike-slip focal mechanisms. These events, which concentrate at upper mantle depths (i.e., between 30 and 60 km depth), appear to be associated with inverted rift structures identified at the transition zones between the different rheological domains that localize regional stresses and hence seismic strain.

Previous works on the 1755 earthquake have proposed a number of candidate sources for this event, such as the GB⁹, MPF^{11,22,24,25}, the subduction beneath Gibraltar²⁶, the SWIM strike-slip faults²⁸, Horseshoe Fault²⁴, São Vicente Fault²⁴ or some composite systems^{22,24}. However, due to either their limited surface areas, their locations and geometry, or both, they do not appear to be capable of accounting for the large seismic moment, the overall reach and energy pattern of the tsunami, as well as the historical recorded amplitudes and arrival times. Among all the proposed candidates, the only tsunami simulation considering far-field observations²⁷ favours a source location in the HAP area.

Almost all existing studies of the 1755 event rely on the comparison with two of the largest recent earthquakes occurred in SW Iberia, the first on 28 February 1969 (M_w 7.9)^{15,37} and the second on 12 February 2007 (M_w 6.0)^{5,38} (Fig. 1 and

Supplementary Table 1). Both earthquakes share the focal mechanism, location and a deep hypocentre, suggesting that they might have been generated by the same fault system. The M_w 7.9 1969 earthquake generated a small tsunami with centimetric wave heights on the SW Portuguese coasts³⁹. For comparison, several metre wave heights were reported in the same area after the 1755 earthquake, indicating that the energy released by this event was much larger than that of the 1969 one (between 15¹³ and 30¹⁹ times larger according to previous works). The analysis of peak ground accelerations estimated from reported intensities of the 1755 earthquake supports a NE–SW oriented reverse dip-slip mechanism³⁷. This would be similar to that of the 17 December 2009 earthquake ($M_w = 5.5$; Supplementary Table 1)³⁷ associated with the MPF, located at the mouth of the SVC where the HAT changes its orientation in depth and would be linked to the MPF (Figs. 1 and 2, and Supplementary Fig. 1).

As stated above, recent work shows evidence for the presence of a deep structure in the HAP³⁰ between the SAP and GB domains with the location and geometry required to be the source of these large earthquakes. This structure was interpreted as a NE–SW trending, NW-verging blind-deep thrust located in the middle of the HAP (Figs. 1 and 2). Although the HAT was initially interpreted to extend to the SVC, the re-analysis of available geophysical data, in combination with recent seismological studies^{5–8,37,38}, suggest that it rather spans from the MPF to the LS (~200 km). Its location and geometry makes it a likely source candidate for part of the deep seismicity recorded by OBS networks in the area (Figs. 1 and 2).

Earthquakes result from stick-slip frictional instability and its frictional behaviour is commonly described by a rate- and state-variable constitutive law⁴⁰. At steady-state, the frictional response depends on a slip velocity-dependent friction parameter. Depending on the sign of this parameter, the material is either velocity strengthening (i.e., earthquakes cannot nucleate and any earthquake propagating there will tend to stop) or velocity weakening (i.e., earthquakes can nucleate and propagate there). This parameter depends on rock lithology, temperature and pressure. For example, granite is velocity weakening below 300 °C and velocity strengthening above, due to the onset of plasticity of quartz, the most ductile mineral in granite. In oceanic basalt, frictional stability is controlled by feldspar transition, which occurs at ~450 °C³². This temperature is typically assumed to mark the downdip limit of inter-plate seismicity in subduction zones.

According to the interpretation of the local controlled-source seismic tomography models³⁰, the HAT separates serpentinized peridotite basement at the NW (GB domain) from oceanic lithosphere at the SE (GC domain), so the deep frictional stability, which concentrates at upper mantle depths, should be controlled by the rheological transition of olivine, which occurs at ~600 °C^{40,41}. Oceanic plate cooling models indicate that this isotherm is located at 50–55 km depth in a ~140 Myr-old lithosphere⁴², in agreement with the location of the deepest earthquakes in the area⁶ (Fig. 2). This pre-eminence of deep seismicity strongly supports that it is controlled by peridotite/serpentinite rheology. The high peridotite rigidity (~70 GPa) and the potential large stress drop, combined with the large downdip extension of the seismogenic layer (>60 km for a 45° thrust), makes that modest-length thrust faults such as the HAT could potentially account for large earthquakes⁵. Therefore, if we assume a focal depth of 50–60 km on peridotite rock (which has a rigidity of ~70 GPa) and an upward propagation over lower rigidity rocks such as serpentinite (for an average rigidity of ~50 GPa), a dip angle of 45° and a realistic slip-to-length ratio of 8.5×10^{-5} , a M_w 8.5+ earthquake like that of the 1755 Lisbon one requires a fault length of just 160–220 km (Fig. 3).

In this rupture scenario, seismic rupture at shallower levels should be controlled by serpentinite, which is more ductile than peridotite. Experimental results show that, at crustal pressure, temperature conditions, serpentinite is velocity strengthening at plate tectonic rates but it is unstable at higher velocities. This means that although serpentinized regions are not a likely site of earthquake nucleation, seismic rupture of deeper earthquakes could propagate through them⁴³. This two-states mechanical behaviour of serpentinite could explain two apparently contradictory observations: the lack of shallow earthquakes in the region^{6–8} and the occurrence of large, occasionally devastating tsunamis requiring shallow slip and substantial seafloor deformation⁴⁴.

Simulation of the tsunami caused by a HAT-like source.

Although multichannel seismic data and TOPAS sub-bottom profiles across the HAT (Fig. 1) do not provide clear evidence of the thrust reaching the seafloor, the OBS records³⁰ show a laterally coherent deep seismic phase consistent with a reflection at a NW-verging structure reaching at least 25–30 km depth, which is interpreted to extend to at least 60 km depth based on seismological data^{5–8,36}. Such a structure can totalize ~16,700 km² of surface area (Figs. 1 and 2, and Supplementary Fig. 1). The controlled-source seismic tomography model shows that the dip of the blind thrust changes with depth, from 20° to 30° from the surface to 25–30 km depth, to 40°–45° deeper than this level, as indicated by focal mechanism solutions of deep seismicity on this area^{5–8,36} (Fig. 2 and Supplementary Fig. 1).

We have used this fault plane as a source for tsunami simulations (Methods), in order to verify if such a feature is compatible with the reported characteristics of the largest tsunamigenic earthquakes in the area, and in particular with those of the 1755 Lisbon one (Fig. 4). To test this, the simulated travel times, amplitudes and tsunami propagation resulting from the HAT source are compared with the available historical records of the 1755 event^{10–14,16–19,27,45–48} and with previous works^{11,26,27} (Figs. 5 and 6, and Supplementary Tables 2 and 3).

The modelled tsunami propagation fits better than any other proposed candidate with the information included in the available historical chronicles (Figs. 4, 5 and 6, and Supplementary Tables 2 and 3). The HAT source scenario reproduces wave arrivals to all locations reported to be hit by the 1755 tsunami including the distant ones such as the Ireland, Great Britain, Newfoundland, Barbados or Brazilian coasts. In addition, it correctly predicts the zones protected from the tsunami impact, such as Vigo in West Iberia or cities like Boston, Baltimore, and New York in the eastern US coast. The bathymetric roughness has an important effect on tsunami propagation, dispersing, amplifying or diminishing the tsunami waves⁴⁹. For instance, and according to our simulation, Vigo was protected from the tsunami by the rias (i.e., sea-inlet or estuary), southern Florida by the Bahamas Banks, and the Madeira Tore-Rise acted as scatter for tsunami energy protecting the US East coast. In contrast, the Madeira island scattered the energy towards the Caribbean, whereas the Great Meteor seamount scattered it towards Brazil.

Comparing arrival times and tsunami amplitude in particular locations is problematic due to the inaccuracy and incompatibility of some arrival times in historical reports. For instance, they indicate a 50 min difference in the arrival time between Lisbon and Porto Novo, which are just 50 km apart, 35 min difference between Penzance and Newlyn, which are 2 km apart, or 30 min difference between Porto Santo and Madeira Islands, which are 50 km apart. Likewise, they report huge wave heights reaching ~15 m in Lisbon, Cadiz, Tangiers and Azores, which are hard to believe^{26,27}. Historical observations contain information on estimated run-up heights (i.e., maximum height of the

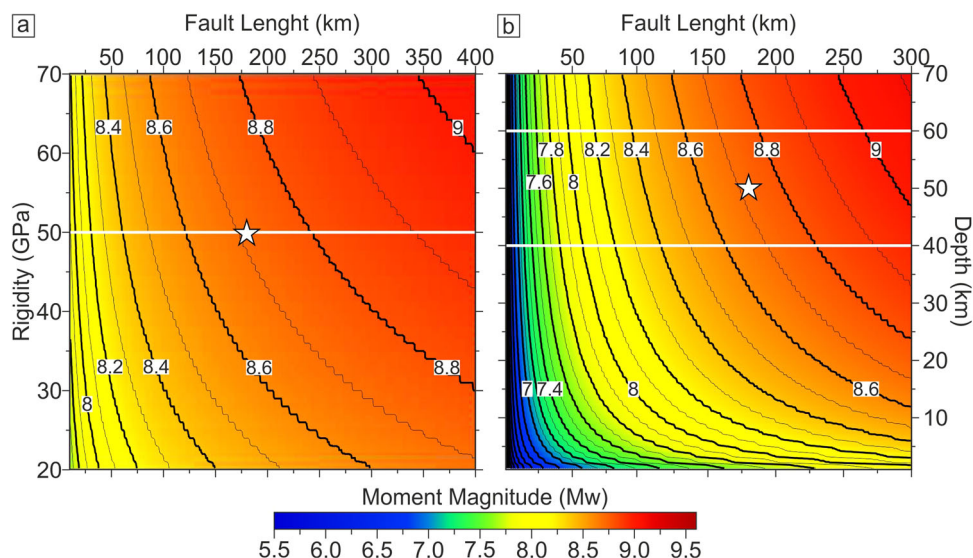


Fig. 3 Moment magnitude (M_w). **a** Calculated earthquake magnitude (M_w) as a function of fault length and rigidity (μ) according to the regional configuration and bulk-rock properties in the SW Iberian margin and tsunami results. White line highlights that assuming a $\mu = 50$ GPa, the generation of a M_w 8.7 earthquake (star) requires a fault length of ~180 km. Slip (15 m), focal depth (50 km) and fault dip (35°) were assumed as constant. **b** Calculated earthquake magnitude (M_w) as a function of fault length and seismogenic depth according to the Horseshoe Abyssal plain Thrust (HAT) geometry, properties and tsunami modelling results. The star locates the M_w value of an earthquake capable of generating a tsunami compatible with that of the 1755 event. White lines highlight the seismogenic zone between 40 and 60 km depth. Rigidity ($\mu = 50$ GPa), slip (15 m) and fault dip (35°) were assumed as constant. See text for further explanations.

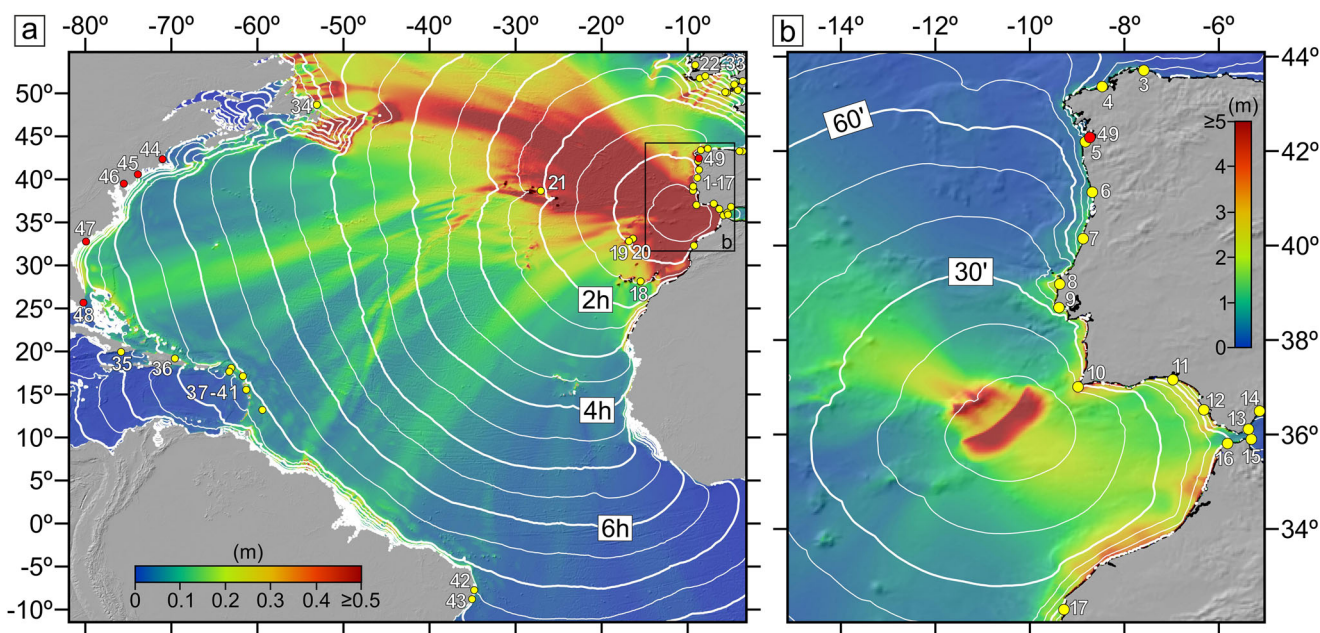


Fig. 4 The HAT tsunami simulation. **a** Tsunami simulation for the Horseshoe Abyssal plain Thrust (HAT) over a regional bathymetric map showing maximum wave heights and tsunami travel time (30 min intervals), and illustrating the effects of bathymetric roughness in tsunami energy propagation. **b** Close-up of the HAT tsunami simulation showing maximum wave heights and tsunami travel times (10 min intervals) highlighting the most affected areas along the SW Iberian and NW Moroccan margins. White numbers refer to localities listed (Id) in Supplementary Tables 2 and 3. Yellow circles label locations of run-up and time arrival reports in Supplementary Tables 2 and 3. Red circles indicate locations with no historical reports.

inundation), but tsunami simulations provide maximum wave height (H_m) before reaching the coast. Therefore, we are comparing different features. To overcome this issue, we have normalized our results to 1 m (\hat{H}_m) below seafloor according to the Green’s Law⁴⁷ (Methods). Almost all previous works^{13,15,21,22} assumed a run-up of 15 m in Cadiz, although the French scientist Louis Godin, who was in Cadiz when the tsunami hit the city, reported a wave height of 5 m⁵⁰. Shallow water estuaries are

highly affected by non-linear propagation effects, which can induce notorious modelling errors. Therefore, we included in our comparison Oerias and Vila Real de San Antonio instead of Lisbon and Huelva (respectively), which are affected by estuaries. Overall, our results fit better than any previous modelled source of the reported observations (Figs. 5 and 6, and Supplementary Tables 2 and 3). In the localities with information available for comparison in the four simulations, the

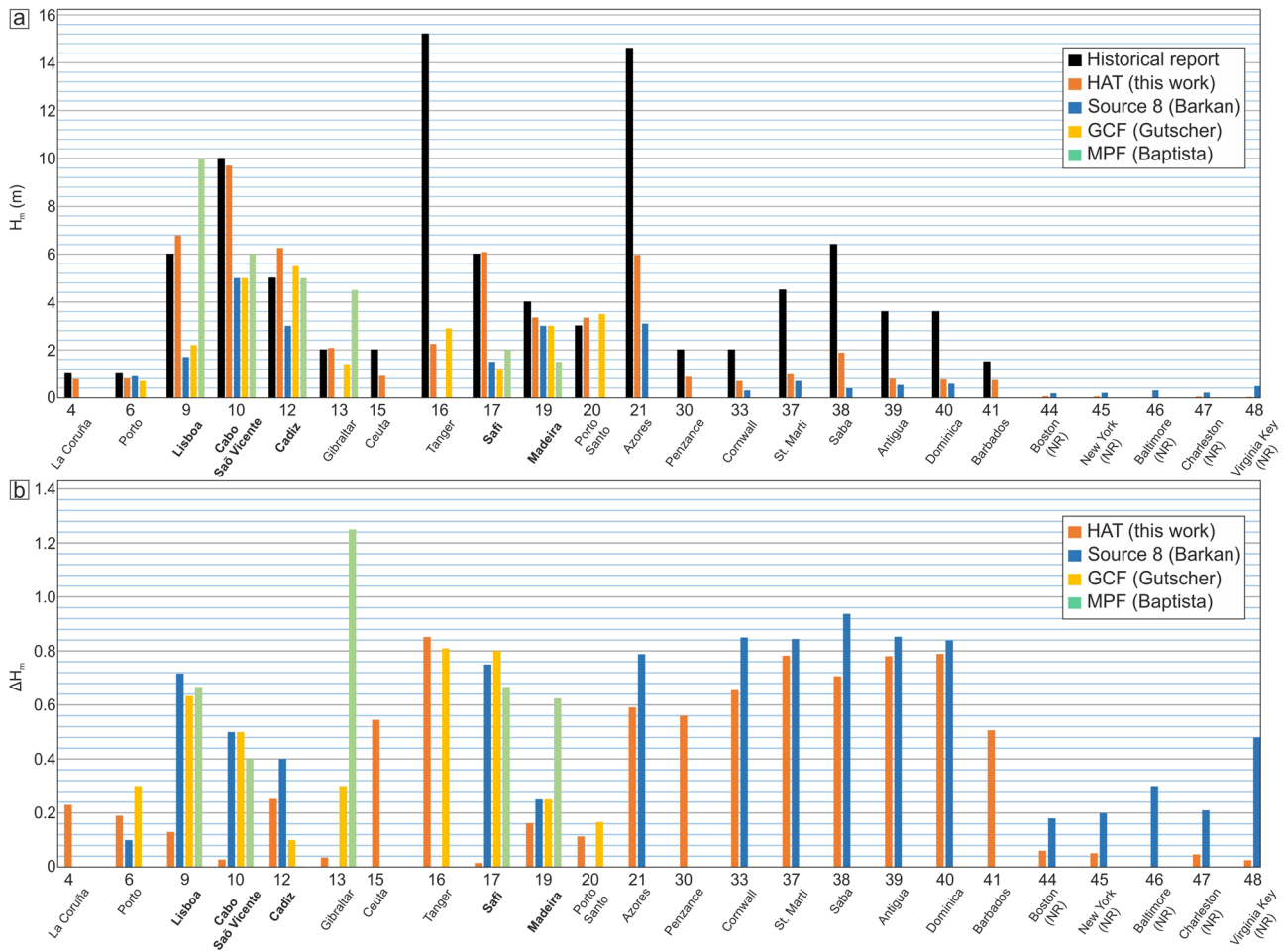


Fig. 5 Comparative between the wave height of the tsunami simulations and the run-up of the 1755 tsunami historical reports. **a** Graph showing the run-up of the 1755 Lisbon tsunami specified on historical reports^{10-14,16-19,27,45-48} (H_m^{obs} in black) and the maximum wave height (H_m^{calc}) obtained from the tsunami simulations of different tectonic structures: the Horseshoe Abyssal plain Thrust (HAT, in orange), the Source 8²⁷ (in blue), the Gulf of Cadiz Fault²⁶ (GCF, in yellow) and the Marques de Pombal Fault¹¹ (MPF, in green) (see Supplementary Table 2). **b** Graph showing the relative variation (ΔH_m) at different locations between the reported run-up (H_m^{obs}) and the H_m^{calc} specified in **a** for each tsunami simulation. In bold are labelled locations with information available for comparison from the four tsunami simulations.

improvement is remarkable (~80%) for the maximum wave heights, whereas the arrival times, which suffer from evident inconsistencies, are comparable or slightly better on average. The HAT modelling results show lower deviations in the estimated wave heights from historical reports in all the reported comparable cases (i.e., 24 localities) except for Porto, Cadiz and Tangier. In the comparison between the only two sources capable of generating transatlantic tsunamis, the HAT always obtains a better fit than Source 8, both in the far- and near-fields (except in Porto, where the difference is minimal). Regarding arrival times, the HAT simulation obtains good results in the far-field, with average differences of <20%, and acceptable results in the near-field, where we obtain values within or close to the reported time range, except in localities with incompatible values for the differential arrival times (i.e., Lisbon, Safi, Madeira and Azores) as also pointed out in previous works^{26,27}. It is noteworthy that only one of the previous works proposed a source capable of generating a transatlantic tsunami and considered near- and far-field historical observations. Their results favour a tsunami generated by a west northwest-east southeast trending fault located in the centre of the HAP²⁷, so that it is at the same location as the HAT but with a different strike direction. However, the proposed orientation was chosen ad hoc for the purposes of the modelling, but it does not correspond to any

known structure in this area and is nearly parallel to the plate convergence direction.

Regional and global implications. In summary, the HAT can explain the location and focal mechanism of the largest instrumental events having occurred in the area, and has the dimensions and the inferred fault-rock bulk properties at focal depths to account for such a giant earthquake. In addition, the tsunami simulation fits better than any other proposed source of the historical reports from the 1755 Lisbon event, particularly the observed wave heights.

Our work has relevant implications at regional level in the fields of active tectonics, petrophysics, seismology and for the seismic and tsunami hazard assessment. We show that the deep regional seismicity is controlled by peridotite/serpentine rheology, allowing modest-length thrust faults to generate anomalously large earthquakes (Fig. 3). This suggests that there is a number of active thrusts in the area^{3,4,25} similar to the HAT that might also have the potential of generating greater earthquakes than previously thought. One example is the GBF, a 155 km-long, NW-verging thrust fault located in between the Tagus and the HAP that thrust two exhumed mantle blocs³² (Fig. 1). Therefore, the earthquake and tsunami hazard associated to these structures must be re-evaluated in light of the new findings.

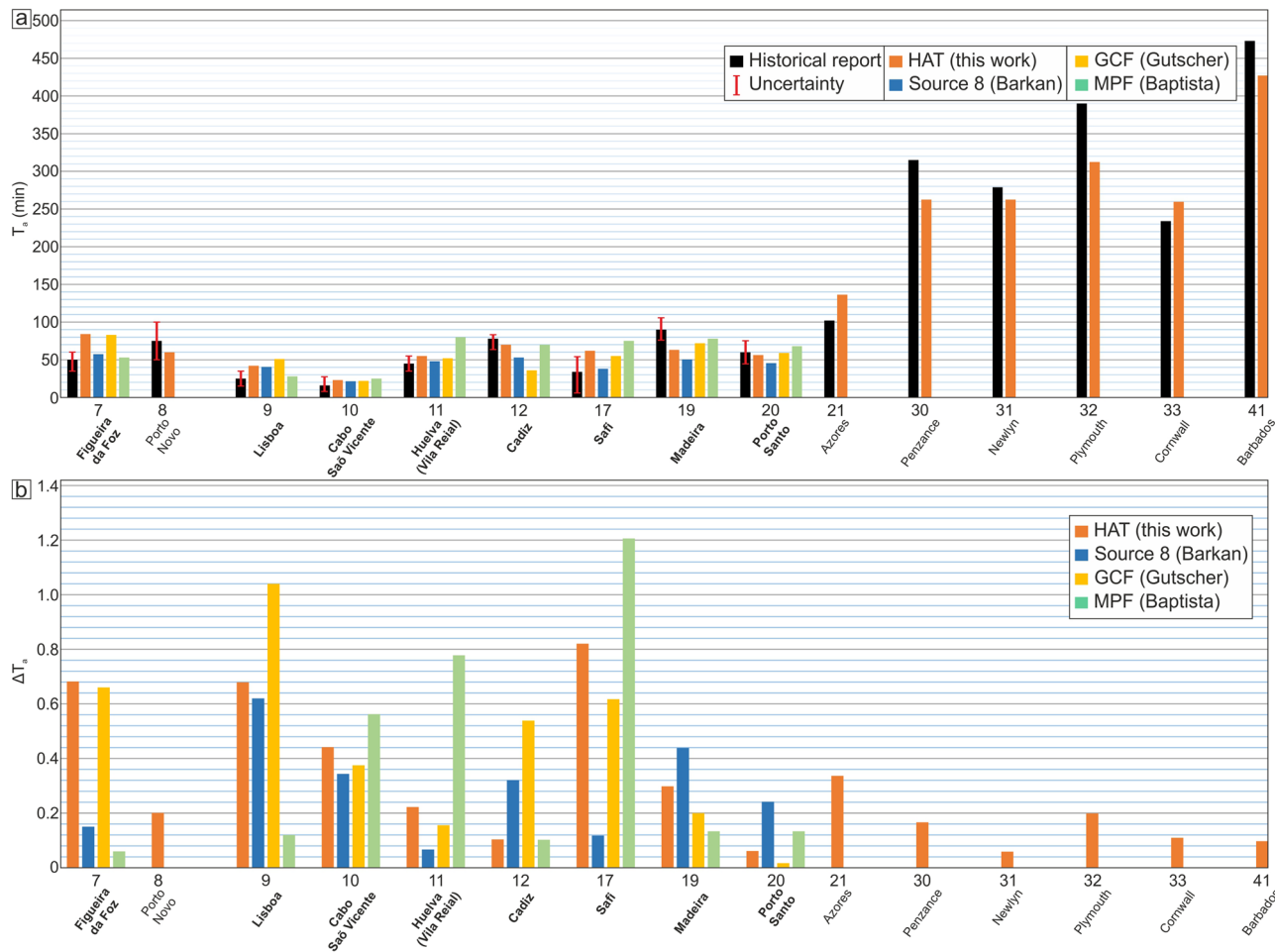


Fig. 6 Comparison between the arrival time of the 1755 tsunami at different locations according to historical reports and those obtained by tsunami simulations. **a** Graph showing the arrival time (t_a^{obs}) and uncertainty of the 1755 Lisbon tsunami specified on historical reports^{10-14,16-19,27,45-48} (black and red error bar, respectively) and the arrival time obtained from the tsunami simulations (t_a^{calc}) of different tectonic structures (HAT in orange, Source 8²⁷ in blue, GCF²⁶ in yellow and MPF¹¹ in green). **b** Relative variation at different locations between the reported TTT and the TTT obtained from tsunami simulations specified in **a**. In bold are labelled locations with information available for comparison from the four tsunami simulations.

Globally, the M_w 8.5+ Lisbon earthquake is a case study evidencing that great destructive tsunamigenic earthquakes can also occur in intra-plate settings (i.e., away from a well-defined plate boundary), challenging the widely extended idea in the scientific community that these events are restricted to subduction zones. There are some recent examples worldwide of great earthquakes in intra-plate settings. The most relevant ones are two large earthquakes of M_w 8.6 and M_w 8.2 associated with modest-length strike-slip faults occurred in the Wharton Basin (Indian Ocean) in April 2012⁵¹. This has been the largest intra-plate earthquake sequence that has been instrumentally recorded⁵². The events initiated ~400 km to the SW of northern Sumatra, Indonesia, on the oceanic side of the Sunda megathrust, within the Wharton Basin and west of the Investigator Fracture Zone⁵¹. According to these authors, the WNW-trending faults experienced large slip and stress drops. The slip was deep and extended into the oceanic mantle (at least up to 60 km depth). The event had such a large magnitude, because these faults experienced very large slip in high-rigidity material⁵¹. Therefore, the occurrence of great earthquakes in intra-plate settings and the possible associated tsunami should be considered in geohazard assessments worldwide.

Methods

Tsunami modelling. To evaluate the seismic and tsunamigenic potential of the HAT and estimate if this structure would generate great earthquakes ($M_w \geq 8.5$)

and transatlantic tsunamis, we first specify fault parameters and physical properties, considering that:

$$M_w = \frac{2}{3} \times \log_{10}(M_0) - 6.07 \tag{1}$$

$$M_0 = \mu \times A \times \bar{D} \tag{2}$$

where M_w is seismic magnitude, M_0 is seismic moment, μ is rigidity, A is fault area and \bar{D} is slip rate. M_0 is 7.16×10^{21} Nm for $M_w = 8.5$. A is 16,730 km² (Supplementary Fig. 1) and μ is 50 GPa. This is an average value assuming that the earthquake nucleated in fresh peridotite at ~50 km depth (~70 GPa) and propagated along the fault plane up to shallower levels where serpentinite and basalts predominate (~30 GPa)⁵. Therefore, the slip value derived from the scaling relations that is required to generate a large earthquake ($M_w = 8.5+$) is 8.5 m. We carried out a succession of tsunami simulations using the HAT fault plane (Supplementary Fig. 1) with a rake of 90°, the parameters described above and varying the slip from 7 to 20 m. Our results show that a slip of 15 m is required to generate a transatlantic tsunami that affects all localities that reported the 1755 event. This value is similar to that assumed in previous works^{9,26,27} (Fig. 3b).

Tsunami simulations, for the equivalent of 12 h of propagation, were performed using the finite-volume Tsunami-HySEA software⁵³. Tsunami-HySEA is a Graphics Processing Unit-optimized code that solves non-linear shallow water equations in spherical or Cartesian coordinate system⁵³. The computational grid has a spatial resolution of 2 arcmin and covers all the Atlantic from Newfoundland to Brazil, considering open boundary conditions. The initial seawater elevation is considered equal to the vertical displacement of the sea bottom, computed as a Volterra’s formulation of the elastic dislocation theory applied to a source buried in an elastic half-space, using the Okada’s fault deformation model⁵⁴. The rupture is considered instantaneous and the initial velocity field is zero. Results of tsunami modelling were processed to obtain regional tsunami wave propagation patterns

and maximum wave height (H_m) profiles at selected coastal points. H_m were extracted at ~50 m depth. They are subsequently extrapolated at the 1 m depth using the Green's law approximation for one-dimensional shoaling as the fourth root of the 50 m, i.e., by applying a multiplicative amplification factor of ~2.66 (Supplementary Table 2). Arrival times at the coast were calculated with the TTT software (<http://www.geoware-online.com/tsunami.html>), using the 2 arcmin digital bathymetry (SRTM15, https://topex.ucsd.edu/WWW_html/srtm15_plus.html), 64 Huygens nodes, and a set of source points on a rectangle obtained from the projection of the fault on the Earth's surface (Supplementary Table 3).

The leading wave of a tsunami is considered to be a shallow water gravity wave, where the ocean depth is negligible compared to the wavelength. In deep waters, the propagation velocity is approximately proportional to $\sqrt{g \times h}$ (3), where g is the acceleration of gravity and h is the water depth in metres. In deep waters, the tsunami wave travels at a velocity of ~800 km/h, whereas at a water depth of 1000 m the velocity drops to 360 km/h. In shallow continental shelf, the wave propagation speed drops dramatically. Under these conditions, an excellent bathymetric grid is required for accurately modelling amplitudes and tsunami arrival times. Due to the enormous dimensions of our tsunami scenario and the unavailability of high-resolution bathymetry for all coastal areas, we used a grid size of 2 arcmin for the simulations.

When comparing modelled results with historical information, it should be considered that some reported observations are incompatible in many cases for any single source, so they are not credible, such as Lisbon, Porto Novo, Penzance or Madeira. In addition, some delays can be due to poorly constrained shallow shelf bathymetry and to the potential effects of landslides (i.e., multiple tsunami sources). However, the turbidite related to the Lisbon earthquake with a thin volume (1.3 km³) is unlikely to have contributed importantly to the 1755 tsunami²⁹. In addition, an increase of 2–3 m should be considered due to the high tide at the time of the tsunami^{27,45,55,56}. In order to facilitate the comparison of results, we have calculated the relative variation of the maximum wave height (ΔH_m) and the arrival time (Δt_a) between the historical values reported (H_m^{obs} and t_a^{obs}) and every simulation (H_m^{calc} and t_a^{calc}) at each location of Tables 2 and 3 (Figs. 5b and 6b).

$$\Delta H_m = \frac{|H_m^{\text{obs}} - H_m^{\text{calc}}|}{H_m^{\text{obs}}} \quad (3)$$

and

$$\Delta t_a = \frac{|t_a^{\text{obs}} - t_a^{\text{calc}}|}{t_a^{\text{obs}}} \quad (4)$$

It is noteworthy that to enable the comparison of results in Fig. 5b, the wave heights have been approached to zero in the localities where the impact of the 1755 tsunami was not reported (identified with "NR" in Table 2 and in Fig. 5).

Data availability

The bathymetric data used for tsunami simulations are available from GEBCO (https://www.gebco.net/data_and_products/gridded_bathymetry_data/). Detailed bathymetry used to generate Figs. 1 and 2 is published in Zitellini et al.²⁸. The epicentral location of the seismicity shown in Fig. 1 is from the IGN Seismic Catalogue (<https://www.ign.es/web/ign/portal/sis-catalogo-terremotos>). The HAT fault plane needed to reproduce the tsunami simulation is available in the figshare repository: <https://doi.org/10.6084/m9.figshare.14589315>.

Code availability

The code necessary to reproduce the Fig. 3 is available in the figshare repository: <https://doi.org/10.6084/m9.figshare.14589315>.

Received: 15 March 2021; Accepted: 1 July 2021;

Published online: 21 July 2021

References

- DeMets, C., Gordon, R. G. & Argus, D. F. Geologically current plate motions. *Geophys. J. Int.* **181**, 1–80 (2010).
- Sartori, R., Torelli, L., Zitellini, N., Peis, D. & Lodolo, E. Eastern segment of the Azores-Gibraltar line (central-eastern Atlantic): an oceanic plate boundary with diffuse compressional deformation. *Geology* **22**, 555–558 (1994).
- Martínez-Loriente, S. et al. Active deformation in old oceanic lithosphere and significance for earthquake hazard: seismic imaging of the Coral Patch Ridge area and neighboring abyssal plains (SW Iberian Margin). *Geochem. Geophys. Geosyst.* **14**, 2206–2231 (2013).
- Martínez-Loriente, S. et al. Morphostructure, tectono-sedimentary evolution and seismic potential of the Horseshoe Fault, SW Iberian Margin. *Basin Res.* **30**, 382–400 (2018).
- Stich, D., Mancilla, F. D. L., Pondrelli, S., & Morales, J. Source analysis of the February 12th 2007, Mw 6.0 Horseshoe earthquake: implications for the 1755 Lisbon earthquake. *Geophys. Res. Lett.* **34** (L12308). <https://doi.org/10.1029/2007GL030012> (2007).
- Geissler, W. H. et al. Focal mechanisms for sub-crustal earthquakes in the Gulf of Cadiz from dense OBS deployment. *Geophys. Res. Lett.* **37**, L18309 (2010).
- Grevenmeyer, I., Matias, L. & Silva, S. Mantle earthquakes beneath the South Iberia continental margin and Gulf of Cadiz – constraints from an onshore-offshore seismological network. *J. Geodyn.* **99**, 39–50 (2016).
- Silva, S. et al. Micro-seismicity in the Gulf of Cadiz: Is there a link between micro-seismicity, high magnitude earthquakes and active faults? *Tectonophysics* **717**, 226–241 (2017).
- Johnston, A. Seismic moment assessment of earthquakes in stable continental regions — III New Madrid 1811–1812, Charleston 1886 and Lisbon 1755. *Geophys. J. Int.* **126**, 314–344 (1996).
- Martínez-Solares, J. M. & López-Arroyo, A. The great historical 1755 earthquake. Effects and damage in Spain. *Journal of Seismology* **8**, 275–294 (2004).
- Baptista, M. A. et al. Constraints on the source of the 1755 Lisbon tsunami inferred from numerical modelling of historical data on the source of the 1755 Lisbon tsunami. *J. Geodyn.* **25**, 159–174 (1998b).
- Lopez-Arroyo, A. & Udias, A. Aftershock sequence and focal parameters of the February 28, 1969 earthquake of the Azores- Gibraltar fracture zone. *Bull. Seism. Soc. Am.* **62**, 699–720 (1972).
- Abe, K. Size of great earthquakes of 1837–1974 inferred from tsunami data. *J. Geophys. Res.* **B4**, 1561–1568 (1979).
- Martins, I. & Mendes-Victor L. A. Contribuição para o estudo da sismicidade de Portugal Continental. Pub. No. 18, p. 67 (Instituto Geofísico do Infante D. Luis. Universidade de Lisboa, Lisboa, Portugal, 1990).
- Fukao, Y. Thrust faulting at a lithospheric plate boundary, the Portugal earthquake of 1969. *Earth Planet. Sci. Lett.* **18**, 205–216 (1973).
- Martínez-Solares, J. M., Lopez, A. & Mezcuca, J. Isoleismal map of the 1755 Lisbon earthquake obtained from Spanish data. *Tectonophysics* **53**, 301–313 (1979).
- Gupta, H. & Gahalaut, V. Three Great Tsunamis: Lisbon (1755), Sumatra-Andaman (2004) and Japan (2011). <https://doi.org/10.1007/978-94-007-6576-4> (Springer Netherlands, 2013).
- Oliveira, C. S. in *Historical Seismology. Modern Approaches in Solid Earth Sciences* (eds. Fréchet, J., Meghraoui, M. & Stucchi, M.) Vol. 2 (Springer, Dordrecht, 2008).
- Baptista, M. A. et al. The 1755 Lisbon earthquake; evaluation of the tsunami parameters. *J. Geodyn.* **25**, 143–157 (1998a).
- Fonseca, J. F. B. D. A reassessment of the magnitude of the 1755 Lisbon earthquake. *Bull. Seismol. Soc. Am.* **110**, 1–17 (2020).
- Chester, D. K. The 1755 Lisbon earthquake. *Prog. Phys. Geogr.* **25**, 363–383 (2001).
- Zitellini, N. et al. Source of the 1755 Lisbon earthquake and tsunami investigated. *EOS Trans. Am. Geophys. Union* **82**, 285 (2001).
- Baptista, M. A., Miranda, J. M., Chierici, F. & Zitellini, N. New study of the 1755 earthquake source based on multi-channel seismic survey data and tsunami modeling. *Nat. Hazards Earth Sci. Syst.* **3**, 333–340 (2003).
- Grácia, E., Danõbeitia, J. J. & Vergés, J., PARSIFAL Team. Mapping active faults offshore Portugal (36°N–38°N): implications for seismic hazard assessment along the southwest Iberian margin. *Geology* **31**, 83–86 (2003).
- Terrinha, P. et al. Tsunamigenic–seismogenic structures, neotectonics, sedimentary processes and slope instability on the southwest Portuguese Margin. *Mar. Geol.* **195**, 55–73 (2003).
- Gutscher, M.-A., Baptista, M. A. & Miranda, J. M. The Gibraltar Arc seismogenic zone: Part 2. Constraints on a shallow east dipping fault plane source for the 1755 Lisbon earthquake provided by tsunami modeling and seismic intensity. *Tectonophysics* **426**, 153–166 (2006).
- Barkan, R., ten Brink, U. S. & Lin, J. Far field tsunami simulations of the 1755 Lisbon earthquake: implications for tsunami hazard to the U.S. East Coast and the Caribbean. *Marine Geology* **264**, 109–122 (2009).
- Zitellini, N. et al. The quest for the Africa-Eurasia plate boundary west of the Strait of Gibraltar. *Earth Planet. Sci. Lett.* **280**, 13–50 (2009).
- Grácia, E. et al. Holocene earthquake record offshore Portugal (SW Iberia): Testing turbidite paleoseismology in a slow convergence margin. *Quat. Sci. Rev.* **29**, 1156–1172 (2010).
- Martínez-Loriente, S. et al. Seismic and gravity constraints on the nature of the basement in the Africa-Eurasia plate boundary: new insights for the geodynamic evolution of the SW Iberian margin. *J. Geophys. Res. Solid Earth* **119**, 127–149 (2014).
- Sallarès, V. et al. Seismic evidence for the presence of Jurassic oceanic crust in the central Gulf of Cadiz (SW Iberia margin). *Earth Planet. Sci. Lett.* **311**, 112–123 (2011).
- Sallarès, V. et al. Seismic evidence of exhumed mantle rock basement at the Gorringe Bank and the adjacent Horseshoe and Tagus abyssal plains (SW Iberia). *Earth Planet. Sci. Lett.* **365**, 120–131 (2013).

33. Srivastava, S. P. et al. Iberian plate kinematics: a jumping plate boundary between Eurasia and Africa. *Nature* **344**, 756–759 (1990).
34. Gràcia, E. et al. Crustal architecture and tectonic evolution of the Gulf of Cadiz (SW Iberian margin) at the convergence of the Eurasian and African plates. *Tectonics* **22**, 1033 (2003b).
35. Terrinha, P. et al. Morphotectonics and strain partitioning at the Iberia–Africa plate boundary from multibeam and seismic reflection data. *Mar. Geol.* **267**, 156–174 (2009).
36. Bartolome, R. et al. Evidence for active strike-slip faulting along the Eurasia–Africa convergence zone: implications for seismic hazard in the SW Iberian Margin. *Geology*. **40**, 495–498 (2012).
37. Buforn, E. et al. Re-evaluation of seismic intensities and relocation of 1969 saint vincent cape seismic sequence: a comparison with the 1755 Lisbon earthquake. *Pure Appl. Geophys.* **177**, 1781–1800 (2020).
38. Lozano, L. et al. A new 3-D P-wave velocity model for the Gulf of Cadiz and adjacent areas derived from controlled-source seismic data: application to nonlinear probabilistic relocation of moderate earthquakes. *Geophys. J. Int.* **221**, 1–19 (2020).
39. Gjevik, B. et al. Modeling tsunamis from earthquake sources near Gorringe Bank southwest of Portugal. *J. Geophys. Res.* **102**, 27931–27949 (1997).
40. Scholz, C. Earthquakes and friction laws. *Nature* **391**, 37–42 (1998).
41. Boettcher, M. S., Hirth, G. & Evans, B. Olivine friction at the base of oceanic seismogenic zones. *J. Geophys. Res.* **112**, B01205 (2007).
42. McKenzie, D., Jackson, J. & Priestley, K. Thermal structure of oceanic and continental lithosphere. *Earth Planet. Sci. Lett.* **233**, 337–349 (2005).
43. Reinen, L. A. Seismic and aseismic slip indicators in serpentinite gouge. *Geology* **28**, 135–138 (2000).
44. Omira, R., Baptista, M. A. & Miranda, J. M. Evaluating tsunami impact on the Gulf of Cadiz Coast (Northeast Atlantic). *Pure Appl. Geophys.* **168**, 1033–1043 (2011).
45. Martínez-Solares, J. M. *Los efectos en España del terremoto de Lisboa (1 de noviembre de 1755)* p. 756 (Dirección General del Instituto Geográfico Nacional, 2001).
46. Lyell, C. *Principles of Geology*. Vol 1, Ch. 25, p. 439 (Williams Cowes, 1830–1833).
47. Allgeyer, S. et al. Could a 1755-like tsunami reach the French Atlantic coastline? Constraints from twentieth century observations and numerical modeling. *Pure Appl. Geophys.* **170**, 1415–1431 (2013).
48. Dawson, A. & Stewart, I. Tsunami geoscience. *Progr. Phys. Geogr. Earth Environ.* **31**, 575–590 (2007).
49. Satake, K. *Tsunamis. Treatise on Geophys.* 2nd Edn, 4, 477–504. <https://doi.org/10.1016/B978-0-444-53802-4.00086-5> (Elsevier, 2015).
50. Witting, J. M. A note on Green's law. *J. Geophys. Res.* **86**, 1995–1999 (1981).
51. Hill, E. M. et al. The 2012 Mw8.6 Wharton Basin sequence: a cascade of great earthquakes generated by near-orthogonal, young, oceanic mantle faults. *J. Geophys. Res. Solid Earth* **120**, 3723–3747 (2015).
52. Yue, H., Lay, T. & Koper, K. En échelon and orthogonal fault ruptures of the 11 April 2012 great intraplate earthquakes. *Nature* **490**, 245–249 (2012).
53. De la Asunción, M. et al. Efficient GPU implementation of a two waves TVD-WAF method for the two-dimensional one layer shallow water system on structured meshes. *Comput. Fluids* **80**, 441–452 (2013).
54. Okada, Y. Surface deformation due to shear and tensile faults in a half-space. *Bull. Seismol. Soc. Am.* **75**, 1135–1154 (1985).
55. Lee, H. S., Shimoyama, T. & Popinet, S. Impacts of tides on tsunami propagation due to potential Nankai Trough earthquakes in the Seto Inland Sea, Japan. *J. Geophys. Res. Oceans*. **120**, 6865–6883 (2015).
56. Androsov A., Behrens J., & Danilov S. in *Computational Science and High Performance Computing IV. Notes on Numerical Fluid Mechanics and Multidisciplinary Design* (eds. Krause E., Shokin Y., Resch M., Kröner D. &

Shokina N.) Vol 115. https://doi.org/10.1007/978-3-642-17770-5_15 (Springer, 2011).

57. IGN Seismic Catalogue. Period: 1960–2020 Available at: <https://www.ign.es/web/ign/portal/sis-catalogo-terremotos>.

Acknowledgements

We are grateful to R. Basili, M. Volpi, F. Maesano, F. Romano and S. Lorito for technical assistance in tsunami simulations, and to C.R. Ranero for the fruitful discussion during the review process. S.M.-L. thanks J. Llopart, H. Perea and A.L. Comeselle for their very helpful comments to improve the figures. This work has been done in the framework of projects FRAME (CTM2015-71766-R) and INSIGHT (CTM2015-70155-R), both funded by the Spanish Plan of Research and Innovation, and has also had funding support of the “Severo Ochoa Centre of Excellence” accreditation (CEX2019-000928-S), of the Spanish Research Agency (AEI). First author's work was done in the framework of the “Juan de la Cierva - Incorporación” fellowship IJCI-2017-33838.

Author contributions

All authors contributed to the conceptualization of the original idea. S.M.-L. led the writing of the paper, conducted the tsunami simulations and made the figures. V.S. contributed to the text and wrote part of the codes of magnitude estimation. E.G. contributed to the text and with funding.

Competing interests

The authors declare no competing interests.

Additional information

Supplementary information The online version contains supplementary material available at <https://doi.org/10.1038/s43247-021-00216-5>.

Correspondence and requests for materials should be addressed to S.M.-L.

Peer review information *Communications Earth & Environment* thanks Andrea Billi, João Duarte Fonseca and the other, anonymous, reviewer(s) for their contribution to the peer review of this work. Primary handling editors: Luca Dal Zilio and Joe Aslin. Peer reviewer reports are available.

Reprints and permission information is available at <http://www.nature.com/reprints>

Publisher's note Springer Nature remains neutral with regard to jurisdictional claims in published maps and institutional affiliations.



Open Access This article is licensed under a Creative Commons Attribution 4.0 International License, which permits use, sharing, adaptation, distribution and reproduction in any medium or format, as long as you give appropriate credit to the original author(s) and the source, provide a link to the Creative Commons license, and indicate if changes were made. The images or other third party material in this article are included in the article's Creative Commons license, unless indicated otherwise in a credit line to the material. If material is not included in the article's Creative Commons license and your intended use is not permitted by statutory regulation or exceeds the permitted use, you will need to obtain permission directly from the copyright holder. To view a copy of this license, visit <http://creativecommons.org/licenses/by/4.0/>.

© The Author(s) 2021